

OPTIMIZED SCHWARZ AND 2-LAGRANGE MULTIPLIER METHODS FOR MULTISCALE PDES *

SÉBASTIEN LOISEL^{††}, HIEU NGUYEN[‡], AND ROBERT SCHEICHL[§]

Abstract. In this article, we formulate and analyze a two-level preconditioner for Optimized Schwarz and 2-Lagrange Multiplier methods for PDEs with highly heterogeneous (multiscale) diffusion coefficients. The preconditioner is equipped with an automatic coarse space consisting of low-frequency modes of the subdomain Dirichlet-to-Neumann maps. Under a suitable change of basis, the preconditioner is a 2×2 block upper triangular matrix with the identity matrix in the upper-left block. We show that the spectrum of the preconditioned system is included in the disk having center $z = 1/2$ and radius $r = 1/2 - \epsilon$, where $0 < \epsilon < 1/2$ is a parameter that we can choose. We further show that the GMRES algorithm applied to our heterogeneous system converges in $O(1/\epsilon)$ iterations (neglecting certain polylogarithmic terms). The number ϵ can be made arbitrarily large by automatically enriching the coarse space. Our theoretical results are confirmed by numerical experiments.

Key words. Domain decomposition, coefficient dependent coarse space, adaptive coarse space enrichment, Dirichlet to Neumann generalized eigenproblem, multiscale PDEs, heterogeneous media

AMS subject classifications. 65N55, 65F10, 65N30, 65N22

1. Introduction. Simulations with heterogeneous media arise naturally in many problems in science and engineering, e.g., modelling of flows in oil reservoirs, porous media, and heat conduction in composite materials [5, 45, 3, 35]. Realistic simulations for such problems often require high-resolution (very fine) meshes. Direct solvers can be expensive for these very large sparse systems of linear equations. In addition, heterogeneity in media can make the associated linear systems severely ill-conditioned and pose a challenge for traditional iterative schemes. Consequently, there has been a lot of research on development of efficient and robust iterative parallel solvers for heterogeneous media, especially in the setting of multigrid, multilevel and domain decomposition methods [9, 19, 23, 1, 20, 39, 48, 47, 15, 16, 31, 40, 42, 6, 41, 44, 43].

Domain decomposition splits a problem into coupled subproblems on smaller subdomains forming a partition of the original domain [36, 46, 30]. It is one of the most popular approaches to solve large-scale problems on parallel supercomputers. In domain decomposition, a coarse grid is an essential ingredient to achieve scalability. Early works, e.g. [4, 10, 9, 23, 46, 29, 48], show that many domain decomposition methods work for heterogeneous media. However, these methods all require a geometric coarse grid which resolves the discontinuities in the properties of the media. In practice, this is a strong requirement as the properties of the media might have complicated variation on many scales and be difficult to capture by a geometric coarse grid. Recently, there have been works on coarse grids that do not resolve the heterogeneity in the media [19, 39, 20, 32], and especially automatic coarse spaces that depend on the properties of the media [15, 16, 31, 40, 42, 6, 41, 44, 43]. In the latter, the coarse spaces are constructed from eigenfunctions associated with small eigenvalues (low-frequency modes) of appropriated generalized eigenvalue problems. They are

*The work of S. Loisel and H. Nguyen was supported by the Numerical Algorithms and Intelligent Software Centre funded by the UK EPSRC grant EP/G036136 and the Scottish Funding Council.

[†]Corresponding Author.

[‡]Department of Mathematics, Heriot-Watt University, Riccarton, Edinburgh, EH14 4AS, United Kingdom. Email: S.Loisel@hw.ac.uk, H.Nguyen@hw.ac.uk

[§]Department of Mathematical Sciences, University of Bath, Bath BA2 7AY, United Kingdom. Email: R.Scheichl@bath.ac.uk

indeed “energy minimizing spaces with constraints” and can be analyzed using the unified theory in [40]. In this paper, we utilize automatic coarse spaces similar to the ones in [31, 6] to formulate an efficient preconditioner for the optimized Schwarz and 2-Lagrange multiplier (2LM) domain decomposition methods.

2LM methods are generalized versions of Optimized Schwarz Methods [18, 17, 26, 27, 11]. They use Robin transmission condition across the “artificial interface” and the Robin parameter can be optimized to obtain the fastest convergence. The first form of 2LM method was introduced in [13] and its relation with Optimized Schwarz Methods was established in [37]. In [24], Loisel gave a rigorous formulation of the methods for general domains and cross points. The methods have been successfully used for different academic and engineering large-scale applications [34, 21, 2].

2LM methods work with a nonoverlapping decomposition. Their formulations are similar to that of the FETI method [14]. However, instead of having local Neumann problems, 2LM methods have local Robin problems (one for each subdomain). The solvability of these Robin problems is guaranteed, thus there is no need for special treatment of floating subdomains as in the FETI method. In 2LM methods, the global linear system is reduced to a system on the interface for the Lagrange multipliers. The 2LM interface system, which is non-symmetric in the considered methods, is of much smaller size but can still be difficult to solve by iterative solvers. One-level and two-level preconditioners for this system were studied in [24, 25]. For the two-level preconditioner, the coarse space is spanned by piecewise constant functions on the trace space. These are indeed eigenfunctions associated with the eigenvalue 0 of the subdomain Dirichlet-to-Neumann (DtN) maps [6]. Under a suitable change of basis, the two-level preconditioner in [25] has a 2×2 block diagonal structure. This preconditioner appears to work well for homogeneous media but its performance deteriorates for heterogeneous media (see numerical experiments in subsections 5.4 and 5.5).

In this work, not only the piecewise constant functions but other low-frequency eigenfunctions of the subdomain DtN maps are also included in the coarse space as suggested by [31, 6]. Our preconditioner is formulated, under a suitable change of basis, as a 2×2 block upper triangular matrix with the identity matrix in the upper-left block. The changes in the coarse space and the form of the preconditioner mean the analysis in [25] is no longer valid. With a new analysis, we are able to show that the spectrum of the preconditioned system, except for the isolated eigenvalue 1, is included in the disk having center $(1/2, 0)$ and radius $1/2 - \epsilon$, where $0 < \epsilon < 1/2$ is a parameter. Under suitable assumptions, this leads to explicit upper bounds for the relative residual norm of the GMRES algorithm. Asymptotically, these bounds decrease to 0 linearly with the same rate at which $(1 - 2\epsilon)^{k-2}$ converges to 0, where k is the iteration number. In addition, the parameter ϵ , and consequently the rate of convergence, can be calculated a priori once a tentative coarse space is chosen. If ϵ is too small (slow convergence), it can be made bigger (faster convergence) by enriching the tentative coarse space with eigenmodes of the subdomain DtN maps associated with the next (larger) frequencies. In other words, the coarse space can be adapted automatically to the variation of the coefficient and the difficulty of the problem to ensure a good rate of convergence.

The rest of this paper is organized as follows. We first state the model problem, derive the 2LM system and introduce the spectral coarse space preconditioner in section 2. In section 3, we discuss the motivations as well as the structure of our preconditioner through studying a transform of the 2LM system. Convergence anal-

ysis and optimal choice of the Robin parameter is given in section 4. In section 5, we present an extensive set of numerical experiments for different types of the diffusion coefficient with different configurations of the mesh size, the number of subdomains and the partition to verify our theoretical results. We end with a short conclusion in section 6.

2. Method formulation.

2.1. Preparatory material. We consider the following model problem

$$(2.1) \quad \begin{aligned} -\nabla \cdot (\alpha(x) \nabla u(x)) &= f(x) & \text{in } \Omega, \\ u(x) &= 0 & \text{on } \partial\Omega, \end{aligned}$$

where the diffusion coefficient $\alpha(x)$ is a positive function that may have large variations within Ω .

Let \mathcal{T}_h be a mesh of size h of Ω . We assume that \mathcal{T}_h resolves any discontinuity in $\alpha(x)$, i.e. $\alpha(x)$ is piecewise constant on \mathcal{T}_h . When (2.1) is discretized, e.g. using piecewise linear finite elements with basis $\{\phi_j\}_{j=1}^n$, we obtain the following system of linear equations

$$(2.2) \quad Au = f.$$

Assume the domain Ω has a nonoverlapping decomposition $\Omega = \cup_{i=1}^p \Omega_i \setminus \partial\Omega$ with the ‘‘artificial interface’’ $\Gamma = \cup_{i=1}^p \partial\Omega_i \setminus \partial\Omega$. The partition can have floating subdomains. Let $H = \max_i \{\text{diam}(\Omega_i)\}$. For each subdomain Ω_i , we consider the local problem

$$(2.3) \quad \begin{aligned} -\nabla \cdot (\alpha(x) \nabla u_i(x)) &= f(x) & \text{in } \Omega_i, \\ (a + \frac{\partial}{\partial n_i}) (\alpha(x) u_i(x)) &= \lambda_i(x) & \text{on } \partial\Omega_i \setminus \partial\Omega, \\ u_i(x) &= 0 & \text{on } \partial\Omega_i \cap \partial\Omega \end{aligned},$$

where $a > 0$ is the ‘‘Robin parameter’’, n_i is the outward normal vector of the boundary $\partial\Omega_i \setminus \partial\Omega$ and λ_i is a Lagrange multiplier.

Multiplying the first equation of (2.3) with a test function $v \in H_0^1(\Omega_i, \partial\Omega_i \cap \partial\Omega)$, applying the divergence theorem and using the second and third equation, we get the variational formulation of the local problem: find $u_i \in H_0^1(\Omega_i, \partial\Omega_i \cap \partial\Omega)$ such that

$$(2.4) \quad \int_{\Omega_i} \alpha(\nabla u_i \cdot \nabla v) dx + a \int_{\partial\Omega_i} \alpha u_i v dx = \int_{\Omega_i} f v dx + \int_{\partial\Omega_i} \lambda_i v dx,$$

for all $v \in H_0^1(\Omega_i, \partial\Omega_i \cap \partial\Omega)$.

Discretizing (2.4) using the finite element method with $\{\phi_j^{(i)}\}_{j=1}^{n_i}$, the subset of the basis associated with Ω_i , we have

$$(2.5) \quad (A^{(i)} + aB^{(i)})u_i = f^{(i)} + \lambda^{(i)},$$

where

$$(2.6a) \quad A_{kl}^{(i)} = \int_{\Omega_i} \alpha(\nabla \phi_l \cdot \nabla \phi_k) dx, \quad B_{kl}^{(i)} = \int_{\partial\Omega_i} \alpha \phi_l \phi_k dx$$

$$(2.6b) \quad f_k^{(i)} = \int_{\Omega_i} f \phi_k dx, \quad \lambda_k^{(i)} = \int_{\partial\Omega_i} \lambda_i \phi_k dx.$$

We would like to find λ_i so that each local discrete solution u_i is the restriction of the global discrete solution u on Ω_i , namely

$$(2.7) \quad R_i u = u_i.$$

Here R_i is the restriction matrix, which restricts any n -dimensional vector u (associated with a grid function on the mesh \mathcal{T}_h of Ω) to an n_i -dimensional vector $R_i u$ that contains only the components of u corresponding to Ω_i .

2.2. 2LM system. Relabelling degrees of freedom (dofs) to separate those in the interior of Ω_i (corresponding to subscript I) and those on the boundary $\partial\Omega_i$ (corresponding to subscript Γ), (2.5) becomes:

$$(2.8) \quad \begin{bmatrix} A_{II}^{(i)} & A_{I\Gamma}^{(i)} \\ A_{\Gamma I}^{(i)} & A_{\Gamma\Gamma}^{(i)} + aB_i \end{bmatrix} \begin{bmatrix} u_I^{(i)} \\ u_\Gamma^{(i)} \end{bmatrix} = \begin{bmatrix} f_I^{(i)} \\ f_\Gamma^{(i)} + \lambda_i \end{bmatrix}.$$

Theoretically, B_i and λ_i are respectively the submatrix and “subvector” of $B^{(i)}$ and $\lambda^{(i)}$ associated only with dofs on $\partial\Omega_i$. However, we will show later in Lemma 2.1 that our method formulation does not rely on the formulation of $B^{(i)}$ in (2.6). Therefore, we let B_i be an arbitrary symmetric positive definite matrix of the appropriated size.

Eliminating the interior unknowns $u_I^{(i)}$ in (2.8), we arrive at the following system for the unknowns on the interface

$$(2.9) \quad (S_i + aB_i)u_\Gamma^{(i)} = g_i + \lambda_i$$

where $S_i = A_{\Gamma\Gamma}^{(i)} - A_{\Gamma I}^{(i)}(A_{II}^{(i)})^{-1}A_{I\Gamma}^{(i)}$ and $g_i = f_\Gamma^{(i)} - A_{\Gamma I}^{(i)}(A_{II}^{(i)})^{-1}f_I^{(i)}$ are the Schur complement and the accumulated right-hand-side, respectively.

Let S and B be the block-diagonal matrices $S = \text{diag}\{S_1, S_2, \dots, S_p\}$ and $B = \text{diag}\{B_1, \dots, B_p\}$. In addition, denote $g = [g_1^T, \dots, g_p^T]^T$, $\lambda = [\lambda_1^T, \dots, \lambda_p^T]^T$ and $u_\Gamma = [u_\Gamma^{(1)T}, \dots, u_\Gamma^{(p)T}]^T$. Since the matrices S_i are symmetric positive semi-definite, the matrices B_i are symmetric positive definite and $a > 0$, the matrices $S_i + aB_i$ are invertible. Therefore, (2.9) is equivalent to

$$(2.10) \quad aBu_\Gamma = Q(g + \lambda),$$

where

$$(2.11) \quad Q = aB(S + aB)^{-1} = \begin{bmatrix} aB_1(S_1 + aB_1)^{-1} & & & \\ & \ddots & & \\ & & \ddots & \\ & & & aB_p(S_p + aB_p)^{-1} \end{bmatrix}.$$

If we think of the vector $[u_1^T, \dots, u_p^T]^T$ as a functions which is defined on Ω , continuous inside each Ω_i , but with jump discontinuities across Γ , then the vector u_Γ is actually its **multi-valued** or **many-sided trace**. For each vertex $x_j \in \Gamma$, let m_j be its multiplicity, namely the number of subdomains adjacent to x_j . In order for u_Γ to correspond to a continuous function, e.g the solution of (2.1), the following relation must hold

$$(2.12) \quad Ku_\Gamma = u_\Gamma,$$

where

$$(2.13) \quad K = \Pi^T \text{diag}\left\{ \frac{1}{m_{j_1}} \mathbf{1}_{m_{j_1} \times m_{j_1}}, \dots, \frac{1}{m_{j_p}} \mathbf{1}_{m_{j_p} \times m_{j_p}} \right\} \Pi,$$

with $\mathbf{1}$ is the matrix of ones, j_k , $1 \leq k \leq n_\Gamma$ are the global indices of the dofs on the interface and Π is the permutation that rearranges these dofs so that they have the same ordering as in u_Γ . Since $K^2 = K$ and $K^T = K$, K is an orthogonal projection (it projects onto the space of continuous many-side trace).

We also need to equate the fluxes of the sub-solutions across the artificial interface Γ . Using ϕ_j , a nodal basis function associated with Γ , as a test function for (2.3), we find that

$$(2.14) \quad \int_{\partial\Omega_i} \alpha \frac{\partial u_i}{\partial n_i} \phi_j dx = \int_{\Omega_i} \alpha (\nabla u_i \cdot \nabla \phi_j) dx - \int_{\Omega_i} f v dx.$$

Consequently, the ‘‘discrete flux vector’’ $\eta^{(i)}$ of the local solution u_i across $\partial\Omega_i$ can be computed by:

$$(2.15) \quad \eta^{(i)} = A_{\Gamma I}^{(i)} u_I^{(i)} + A_{\Gamma \Gamma}^{(i)} u_\Gamma^{(i)} - f_\Gamma^{(i)} = \lambda_i - a B_i u_\Gamma^{(i)} \quad (\text{using (2.8)}).$$

The discrete weighted fluxes are matched when $\sum_{i=1}^p R_i^T [0 \ \eta^{(i)T}]^T = 0$, or equivalently

$$(2.16) \quad a B u_\Gamma = \lambda.$$

The following result is purely algebraic, namely (2.2) and (2.6) do not need to come from (2.1).

LEMMA 2.1. *Let us assume that A is invertible, $A = \sum_{i=1}^p R_i^T A^{(i)} R_i$ and $f = \sum_{i=1}^p R_i^T f_i$. We also assume that the matrices on the left hand side of (2.8) are invertible. Then there exists a unique solution $u_1, \dots, u_p, \lambda_1, \dots, \lambda_p$ to the simultaneous equations (2.8), (2.12) and (2.16). Such solution u_1, \dots, u_p implies the unique solution u of (2.2) through (2.7) and vice versa.*

Proof. Assume u is the unique solution of (2.2). Let $u_i = R_i u$ and substitute them into (2.8) we obtain λ_i . Clearly, (2.12) holds. In addition,

$$(2.17) \quad \begin{aligned} Au &= \sum_{i=1}^p R_i^T A^{(i)} R_i u = \sum_{i=1}^p R_i^T A^{(i)} u_i = \sum_{i=1}^p R_i^T (f^{(i)} + \lambda^{(i)} - a B^{(i)} u_i) \\ &= f + \sum_{i=1}^p R_i^T \begin{bmatrix} 0 \\ \lambda_i - a B_i u_\Gamma^{(i)} \end{bmatrix}. \end{aligned}$$

This implies (2.16).

Now assume that $u_1, \dots, u_p, \lambda_1, \dots, \lambda_p$ is a solution to the simultaneous equations (2.8), (2.12) and (2.16). As (2.12) holds, there is clearly a unique u that satisfies (2.7). The fact that this u is also the solution of (2.2) comes from arguments in (2.17).

If $u_1^*, \dots, u_p^*, \lambda_1^*, \dots, \lambda_p^*$ is another solution to the simultaneous equations (2.8), (2.12) and (2.16). From (2.8), if $u_i^* = u_i$ then $\lambda_i^* = \lambda$. If $u_i^* \neq u_i$ for some $1 \leq i \leq p$, we then obtain u^* satisfying (2.7) and consequently $Au^* = f$. Since A is invertible, $u^* = u$. Hence $u_i^* = R_i u^* = R_i u = u$ which contradicts $u_i^* \neq u_i$. \square

REMARK 2.2. *We again emphasize that the result in Lemma 2.1 is purely algebraic. Especially, $B^{(i)}$, and thus B_i do not need to come from (2.1), i.e. they do not have to be defined as in (2.6).*

As there is freedom in choosing B_i , we make the following assumption.

ASSUMPTION 2.3. *The matrices B and K commute, i.e.,*

$$KB = BK.$$

In fact, we will choose B to be the diagonal matrix satisfying

$$(2.18) \quad \text{diag}(B) = K \text{diag}(\bar{B}),$$

where $\bar{B} = \text{diag}\{\bar{B}_1, \dots, \bar{B}_p\}$, with \bar{B}_i being the lumped mass matrix on $\partial\Omega_i$. In other words, B is the ‘‘average’’ of the lumped mass matrix associated with dofs on the interface. In some sense, our choice of B means that the interface mass matrix and the local generalized eigenproblem introduced later in (3.5) take into account some information about the behaviour of the coefficient in the vicinity of the interface in adjacent subdomains.

Using Assumption 2.3, equations (2.16), (2.12) and (2.10), after some algebra, we find the non-symmetric 2LM system

$$(2.19) \quad A_{2LM}\lambda := (I - 2K)(Q - K)\lambda = -(I - 2K)Qg.$$

The 2LM system (2.19) can be regarded as a generalization of Optimized Schwarz methods to the case where the partition has cross points (cf. [24, 25]).

2.3. The spectral coarse space preconditioner. The system (2.19) can be solved iteratively using GMRES [38]. In order to accelerate the convergence of GMRES, we now briefly introduce a preconditioner with a spectral coarse space. Its motivations and derivation will be given in detail in section 3.

In the homogeneous case [25], the coarse space would consist of the kernel of S (i.e. the piecewise constant functions). When the problem is heterogeneous, we use the same piecewise constant functions, as well as any functions that are ‘‘almost’’ in the kernel of S .

We choose a ‘‘truncation parameter’’ s_{\min} for the coarse space, and we consider all the generalized eigenvectors

$$Sv = sBv \text{ where } s < s_{\min}.$$

We collect all such column vectors into the columns of a matrix J , which is B -orthonormalized

$$J^T B J = I.$$

We define the B^{-1} -orthogonal projection $E = B J J^T$ and the spectral coarse space preconditioner by

$$(2.20) \quad P = (I - E) + A_{2LM}E.$$

The preconditioned system is

$$(2.21) \quad P^{-1}A_{2LM}\lambda = -P^{-1}(I - 2K)Qg$$

An efficient strategy for evaluating the matrix-vector product $P^{-1}\lambda$ is as follows (see subsection 3.3 for explanation). Let

$$(2.22) \quad Z = J^T A_{2LM} B J$$

be the ‘‘coarse matrix’’. Then,

$$(2.23) \quad \begin{aligned} P^{-1} &= (I + (I - E)A_{2LM}E)(I - E + B J Z^{-1} J^T) \\ &= (I + (I - B J J^T)A_{2LM} B J J^T)(I - B J J^T + B J Z^{-1} J^T). \end{aligned}$$

The size of the coarse matrix Z (also the number of columns of the matrix J) is the number of coarse basis functions, which depends on our choice of s_{\min} and on the inherent physical difficulty of the underlying problem. In general, this number is much smaller than the size of the 2LM system. This ensures that P is competitive in term of computational cost.

3. Transformed 2LM system.

3.1. The transformation. It is clear from (2.11) that Q is non-symmetric. In order to exploit symmetry in our analysis, we consider the following similarity transformation.

DEFINITION 3.1. *Given a matrix C , a vector v , we define their “hat-associates”:*

$$(3.1) \quad \hat{C} := B^{-1/2}CB^{1/2}, \quad \hat{v} := B^{-1/2}v.$$

Here we note that $B^{1/2}$ and $B^{-1/2}$ are well-defined because B is a diagonal matrix with positive entries.

REMARK 3.2. $\sigma(C) = \sigma(\hat{C})$, where $\sigma(\cdot)$ denotes the spectrum of a matrix.

Multiplying (2.19) with $B^{-1/2}$ from the left, and using the fact that $B^{1/2}$ and K commute, we obtain the transformed 2LM system

$$(3.2) \quad \hat{A}_{2LM}\hat{\lambda} = (I - 2K)(\hat{Q} - K)\hat{\lambda} = -(I - 2K)\hat{Q}\hat{g}.$$

Using the definition of Q in (2.11), it follows that

$$\hat{Q} = B^{-1/2}QB^{1/2} = B^{-1/2}aB(S + aB)^{-1}B^{1/2} = a(B^{-1/2}SB^{-1/2} + aI)^{-1}.$$

Clearly, \hat{Q} is symmetric. In addition,

$$(3.3) \quad \sigma(Q) = \sigma(\hat{Q}) = \left\{ \frac{a}{a+s} \mid s \in \sigma(B^{-1/2}SB^{-1/2}) \right\}.$$

Furthermore, the spectrum of $\check{S} = B^{-1/2}SB^{-1/2}$ is exactly the same as the spectrum of the following generalized eigenvalue problem:

$$(3.4) \quad Sv = sBv.$$

Due to the block-structure of S and B , the spectrum of (3.4) is the union of the spectra of the following sub-generalized eigenvalue problems on the subdomains:

$$(3.5) \quad S_i v^{(i)} = s B_i v^{(i)}.$$

As S_i is symmetric positive semi-definite and B_i is symmetric positive definite, all the eigenvalues of (3.5) are non-negative. In addition, when Ω_i is a floating subdomain, (3.5) has exactly one eigenvalue that is 0 with constant eigenvectors. This together with (3.3), (3.4) and (3.5) imply that

$$(3.6) \quad \sigma(\hat{Q}) = \sigma(Q) \subset (0, 1].$$

According to [6], if B_i is the submatrix of $B^{(i)}$ associated with dofs on $\partial\Omega_i$ and is computed exactly as in (2.6) then (3.5) is the discrete form of the following eigenproblem in function space

$$(3.7) \quad \text{DtN}_i(v_\Gamma^{(i)}) = s \alpha v_\Gamma^{(i)}, \quad \text{where } \text{DtN}_i(v_\Gamma^{(i)}) = \alpha \frac{\partial v^{(i)}}{\partial n_i} \Big|_{\partial\Omega_i \setminus \partial\Omega}$$

and $v^{(i)}$ is the α -harmonic extension of $v_{\Gamma}^{(i)}$ to Ω_i . The coarse spaces in [31, 6] are spanned by eigenfunctions associated with low-frequency modes of (3.7). We use the same type of coarse space but with B_i being the ‘‘averaged’’ lumped mass matrix on the boundary (cf. (2.18)). In other words, the α in (3.7) at each dof on $\Gamma \cap \partial\Omega_i$ is replaced by its domain-wise averaged counterpart.

3.2. Block structure of the preconditioner. Assume $\sigma(\hat{Q}) = \sigma(Q) = [\epsilon, 1 - \epsilon] \cup (1 - \epsilon, 1]$, where $0 < \epsilon < 1/2$. Then the coarse space \hat{V}_0 is defined as the subspace spanned by eigenvectors of \hat{Q} corresponding to the eigenvalues in the interval $(1 - \epsilon, 1]$ (these eigenvalues correspond to the small eigenvalues of (3.5) and (3.7)). Let \hat{J} be a matrix whose columns are orthonormal eigenvectors of \hat{Q} spanning \hat{V}_0 . Also let

$$\hat{E} = \hat{J}\hat{J}^T,$$

i.e., \hat{E} is the orthogonal projection onto the coarse space \hat{V}_0 . We define our preconditioner for the transformed 2LM system (3.2) as follows

$$(3.8) \quad \hat{P} = (I - \hat{E}) + \hat{A}_{2LM}\hat{E}.$$

Under a suitable change of basis, the matrices \hat{Q} and K have the following forms

$$(3.9) \quad \hat{Q} = \begin{bmatrix} \hat{Q}_1 & O \\ O & \hat{Q}_2 \end{bmatrix} \text{ and } K = \begin{bmatrix} K_{11} & K_{12} \\ K_{21} & K_{22} \end{bmatrix},$$

where \hat{Q}_1 , \hat{Q}_2 and K are symmetric with $\sigma(\hat{Q}_1) \subset [\epsilon, 1 - \epsilon]$, $\sigma(\hat{Q}_2) \subset (1 - \epsilon, 1]$, $\sigma(K) = \{0, 1\}$. Under this permutation, we find that the transformed 2LM matrix is

$$(3.10) \quad \hat{A}_{2LM} = \begin{bmatrix} (I - 2K_{11})\hat{Q}_1 + K_{11} & -2K_{12}\hat{Q}_2 + K_{12} \\ -2K_{21}\hat{Q}_1 + K_{21} & (I - 2K_{22})\hat{Q}_2 + K_{22} \end{bmatrix},$$

the projection is

$$(3.11) \quad \hat{E} = \begin{bmatrix} O & O \\ O & I \end{bmatrix},$$

and the preconditioner is

$$(3.12) \quad \hat{P} = \begin{bmatrix} I & -2K_{12}\hat{Q}_2 + K_{12} \\ O & (I - 2K_{22})\hat{Q}_2 + K_{22} \end{bmatrix}.$$

It can be seen that the preconditioner \hat{P} is a 2×2 block upper triangular matrix which is obtained from \hat{A}_{2LM} (cf. (3.10)) by ‘‘zeroing out’’ the lower-left block and replacing the top-left block by I .

3.3. Connection with the original 2LM system. The preconditioned transformed 2LM system is

$$(3.13) \quad \hat{P}^{-1}(I - 2K)(\hat{Q} - K)\hat{\lambda} = \hat{P}^{-1}(I - 2K)\hat{Q}\hat{g}.$$

Multiplying (3.13) from the left by $B^{1/2}$, using Definition 3.1, the fact that K and $B^{1/2}$ commute and $B^{-1/2}B^{1/2} = I$, it yields

$$(3.14) \quad B^{1/2}\hat{P}^{-1}B^{-1/2}(I - 2K)(Q - K)\lambda = -B^{1/2}\hat{P}^{-1}B^{-1/2}(I - 2K)Qg.$$

This implies that using \hat{P} as the preconditioner for the transformed system (3.2) is equivalent with using $P = B^{1/2}\hat{P}B^{-1/2}$ as the preconditioner for the original 2LM system (2.19). In addition, $\sigma(P^{-1}A_{2LM}) = \sigma(\hat{P}^{-1}\hat{A}_{2LM})$.

Using the definition of \hat{P} in (3.2), we recover the formulation of P

$$(3.15) \quad P = B^{1/2}\hat{P}B^{-1/2} = B^{1/2}(I - \hat{E}) + \hat{A}_{2LM}\hat{E}B^{-1/2} = (I - E) + A_{2LM}E,$$

where

$$E = B^{1/2}\hat{E}B^{-1/2} = B^{1/2}\hat{J}\hat{J}^TB^{-1/2} = BJJ^T, \quad J = B^{-1/2}\hat{J}.$$

In addition, if \hat{v} is a normalized eigenvector of \hat{Q} (a column of \hat{J}) then $B^{-1/2}\hat{v}$ is an eigenvector the generalized eigenvalue problem (3.4). Furthermore, as the columns of \hat{J} are orthonormal, the columns of J are orthonormal with respect to the B -norm:

$$J^TBJ = \hat{J}^T\hat{J} = I.$$

These explain the formulation of our spectral coarse space preconditioner given in advance in section 2.

We now explain how to efficiently compute the matrix-vector product $\hat{P}^{-1}\hat{\lambda}$. First, we note that Z is the lower-right block of \hat{P} and \hat{A}_{2LM} :

$$(3.16) \quad \begin{aligned} Z &= J^T A_{2LM} B J = J^T B^{1/2} \hat{A}_{2LM} B^{-1/2} B J = \hat{J}^T \hat{A}_{2LM} \hat{J} \\ &= (I - 2K_{22})\hat{Q}_2 + K_{22}. \end{aligned}$$

Then consider \hat{P} given by (3.12), we find that

$$(3.17) \quad \begin{aligned} \hat{P}^{-1} &= \begin{bmatrix} I & -2K_{12}\hat{Q}_2 + K_{12} \\ O & I \end{bmatrix} \begin{bmatrix} I & O \\ O & Z^{-1} \end{bmatrix}, \\ &= (I + (I - \hat{E})\hat{A}_{2LM}\hat{E})(I - \hat{E} + \hat{J}Z^{-1}\hat{J}^T) \\ &= (I + (I - \hat{J}\hat{J}^T)\hat{A}_{2LM}\hat{J}\hat{J}^T)(I - \hat{J}\hat{J}^T + \hat{J}Z^{-1}\hat{J}^T). \end{aligned}$$

Conjugating by $B^{1/2}$ gives P^{-1} in (2.23).

4. Convergence Analysis.

We first study the transformed 2LM system.

LEMMA 4.1. *\hat{P} is invertible if and only if $\hat{Q}_2 - K_{22}$ is invertible. In that case, the spectrum of the preconditioned system $\hat{P}^{-1}\hat{A}_{2LM}$, except for the isolated eigenvalue 1, is included in the disk having center $(1/2, 0)$ and radius $1 - \epsilon$, i.e.,*

$$(4.1) \quad \sigma(\hat{P}^{-1}\hat{A}_{2LM}) \subset \{z \in \mathbb{C} : |z - 1/2| \leq 1/2 - \epsilon\} \cup \{1\} =: S_\epsilon.$$

Proof. We refer the reader to [25, Remark 4] for the invertibility of $\hat{Q}_2 - K_{22}$. Now we only need to show that (4.1) holds.

Since $K^2 = K$, it implies that $(I - 2K)^{-1} = I - 2K$. Thus, for any $\theta \in \mathbb{C}$, we have

$$(4.2) \quad \begin{aligned} \text{rank} \left(\hat{P}^{-1}\hat{A}_{2LM} - \theta I \right) &= \text{rank} \left(\hat{A}_{2LM} - \theta \hat{P} \right) \\ &= \text{rank} \left((I - 2K)(\hat{Q} - K) - \theta(I - \hat{E}) - \theta(I - 2K)(\hat{Q} - K)\hat{E} \right) \\ &= \text{rank} \left((\hat{Q} - K) - \theta(I - 2K)(I - \hat{E}) - \theta(\hat{Q} - K)\hat{E} \right) \\ &= \text{rank} \left(\begin{bmatrix} \hat{Q}_1 - K_{11} - \theta(I - 2K_{11}) & (\theta - 1)K_{12} \\ (\theta - 1)K_{21} & (1 - \theta)(\hat{Q}_2 - K_{22}) \end{bmatrix} \right). \end{aligned}$$

The number θ is an eigenvalue of $\hat{P}^{-1}\hat{A}_{2LM}$ if and only if the rank of $\hat{P}^{-1}\hat{A}_{2LM} - \theta I$ is deficient. This obviously occurs when $\theta = 1$. Let's now consider the case $\theta \neq 1$. Note that the matrix (4.2) has an invertible lower-right block so we can use a Schur complement and study the rank deficiency of the matrix

$$(4.3) \quad W = \left(\hat{Q}_1 - K_{11} - \theta(I - 2K_{11}) + (2\theta - 1)K_{12} \left(\hat{Q}_2 - K_{22} \right)^{-1} K_{21} \right).$$

Setting $\theta = \frac{1}{2} + s$ and $\hat{Q}_1 = \frac{1}{2}I + M$, we find that

$$(4.4) \quad W = M + sG, \quad \text{where } G = \left(2 \left(K_{12} \left(\hat{Q}_2 - K_{22} \right)^{-1} K_{21} + K_{11} \right) - I \right).$$

We assume that

$$(4.5) \quad \sigma(G) \subset (-\infty, -1] \cup [1, \infty).$$

According to (4.2), (4.3) and (4.4), $\theta \neq 1$ is an eigenvalue of $\hat{P}^{-1}\hat{A}_{2LM}$ only if $\sigma(M + sG) \ni 0$. This only happens when

$$(4.6) \quad |\theta - 1/2| = |s| \leq 1/2 - \epsilon,$$

because of Lemma 3 in [8] and the fact that $\sigma(M) = [\epsilon - 1/2, 1/2 - \epsilon]$. The desired relation follows immediately.

Now we need to show that the assumption (4.5) is actually true. Let $K = \begin{bmatrix} U \\ V \end{bmatrix} \begin{bmatrix} U^T & V^T \end{bmatrix}$ with $U^T U + V^T V = I$. The Woodbury identity gives

$$(4.7) \quad \begin{aligned} K_{12} \left(\hat{Q}_2 - K_{22} \right)^{-1} K_{21} + K_{11} &= UV^T (\hat{Q}_2 - VV^T)^{-1} VU^T + UU^T \\ &= U \left(V^T (\hat{Q}_2 - VV^T)^{-1} V + I \right) U^T \\ &= U (I - V^T \hat{Q}_2^{-1} V)^{-1} U^T =: F. \end{aligned}$$

Applying Woodbury's identity one more time, we have

$$\begin{aligned} (I - 2F)^{-1} &= \left(I - 2U(I - V^T \hat{Q}_2^{-1} V)^{-1} U^T \right) \\ &= I - (-2U) \left(I - V^T \hat{Q}_2^{-1} V + (-2U)U^T \right)^{-1} U^T \\ &= I + 2U(I - V^T \hat{Q}_2^{-1} V - 2U^T U)^{-1} U^T \\ &= I - 2U(V^T (\hat{Q}_2^{-1} - I)V + U^T U)^{-1} U^T \leq I. \end{aligned}$$

Furthermore, note that $U(V^T (\hat{Q}_2^{-1} - I)V + U^T U)^{-1} U^T \leq P_U$, where P_U is the orthogonal projection onto the range of U , and hence $(I - 2F)^{-1} \geq -I$. This completes the proof. \square

LEMMA 4.2. *Let $R(\theta) = (\hat{P}^{-1}\hat{A}_{2LM} - \theta I)^{-1}$. Then, for $\theta \notin S_\epsilon$ the resolvent norm is bounded by*

$$(4.8) \quad \|R(\theta)\| \leq \frac{|1 - \theta| + |\theta - \frac{1}{2}| - \frac{1}{2} + \epsilon + (1 - 2\epsilon)\|Z^{-1}\|}{|1 - \theta| \left(|\theta - \frac{1}{2}| - \frac{1}{2} + \epsilon \right)}$$

$$(4.9) \quad =: R_b(\theta).$$

Proof. Performing block-row eliminations on (3.12), we find that

$$\begin{bmatrix} I & O \\ O & ((I - 2K_{22})\hat{Q}_2 + K_{22})^{-1} \end{bmatrix} \hat{P} = \begin{bmatrix} I & -2K_{12}\hat{Q}_2 + K_{12} \\ O & I \end{bmatrix}$$

$$\begin{bmatrix} I & 2K_{12}\hat{Q}_2 - K_{12} \\ O & I \end{bmatrix} \begin{bmatrix} I & O \\ O & ((I - 2K_{22})\hat{Q}_2 + K_{22})^{-1} \end{bmatrix} \hat{P} = I$$

Hence,

$$\hat{P}^{-1} = \begin{bmatrix} I & (2K_{12}\hat{Q}_2 - K_{12})((I - 2K_{22})\hat{Q}_2 + K_{22})^{-1} \\ O & ((I - 2K_{22})\hat{Q}_2 + K_{22})^{-1} \end{bmatrix}.$$

This together with (3.10) implies that the preconditioned matrix $\hat{P}^{-1}\hat{A}_{2LM}$ is

$$\begin{bmatrix} (I - 2K_{11})\hat{Q}_1 + K_{11} + (2K_{12}\hat{Q}_2 - K_{12})((I - 2K_{22})\hat{Q}_2 + K_{22})^{-1}(K_{21} - 2K_{21}\hat{Q}_1) & O \\ ((I - 2K_{22})\hat{Q}_2 + K_{22})^{-1}(K_{21} - 2K_{21}\hat{Q}_1) & I \end{bmatrix}.$$

We now simplify the top-left and bottom-left blocks of the preconditioned matrix using $\hat{Q}_1 = \frac{1}{2}I + M$ where $\|M\| \leq \frac{1}{2} - \epsilon$, which gives:

$$(\hat{P}^{-1}\hat{A}_{2LM})_{11} = \frac{1}{2}I + \left(I - 2K_{11} - 2K_{12}(2\hat{Q}_2 - I)((I - 2K_{22})\hat{Q}_2 + K_{22})^{-1}K_{21} \right) M.$$

We use the Woodbury identity to compute the inverse

$$\begin{aligned} & (I + V^T(2\hat{Q}_2 - I)((I - 2VV^T)\hat{Q}_2 + VV^T)^{-1}V)^{-1} \\ &= I - V^T(2\hat{Q}_2 - I)((I - 2VV^T)\hat{Q}_2 + VV^T) + VV^T(2\hat{Q}_2 - I)^{-1}V \\ &= I - V^T(2I - \hat{Q}_2^{-1})V. \end{aligned}$$

This leads to

$$(\hat{P}^{-1}\hat{A}_{2LM})_{11} = \frac{1}{2}I + \left(I - 2U \left(I - V^T(2I - \hat{Q}_2^{-1})V \right)^{-1} U^T \right) M =: \frac{1}{2}I + YM.$$

In order to save space, we set $X := \hat{P}^{-1}\hat{A}_{2LM}$ such that

$$R(\theta) = \begin{bmatrix} X_{11} - \theta I & 0 \\ X_{21} & (1 - \theta)I \end{bmatrix}^{-1} = \begin{bmatrix} (X_{11} - \theta I)^{-1} & 0 \\ -(1 - \theta)^{-1}X_{21}(X_{11} - \theta I)^{-1} & (1 - \theta)^{-1}I \end{bmatrix}.$$

Using the triangle inequality, it follows that

$$(4.10) \quad \|R(\theta)\| \leq \|(X_{11} - \theta I)^{-1}\| + \|(1 - \theta)^{-1}I\| + \|(1 - \theta)^{-1}X_{21}(X_{11} - \theta I)^{-1}\|.$$

We begin with the upper-left block $R_{11}(\theta) = (X_{11} - \theta I)^{-1}$. We find that $\|YM\| = \|R_{11}(1/2)\| \leq \|M\| \leq \frac{1}{2} - \epsilon$ and hence

$$\sigma_{\min}((1/2 - \theta)I + YM) \geq |1/2 - \theta| - (1/2 - \epsilon).$$

In other words,

$$(4.11) \quad \|R_{11}(\theta)\| \leq \frac{1}{|\theta - \frac{1}{2}| - \frac{1}{2} + \epsilon} \text{ for } |\theta - \frac{1}{2}| > \frac{1}{2} - \epsilon.$$

We now look at the lower-left entry $R_{21}(\theta)$ and find

$$(4.12) \quad R_{21}(\theta) = -2(1-\theta)^{-1}((I-2K_{22})\hat{Q}_2 + K_{22})^{-1}K_{21}M(R_{11}(\theta))$$

From (4.12), (4.11), (3.16) and the fact that $\|M\| \leq 1/2 - \epsilon$, we have

$$(4.13) \quad \begin{aligned} \|R_{21}(\theta)\| &\leq 2|1-\theta|^{-1}\|(I-2K_{22})\hat{Q}_2 + K_{22})^{-1}\| \|K_{21}M\| \|R_{11}(\theta)\| \\ &\leq \left(\frac{1-2\epsilon}{|1-\theta|(|\theta-\frac{1}{2}|-\frac{1}{2}+\epsilon)} \right) \|Z^{-1}\|. \end{aligned}$$

Then the resolvent norm estimate (4.8) follows from (4.10), (4.11) and (4.13). \square

We now state the main convergence result for the transformed 2LM system.

THEOREM 4.3. *Let $\hat{C}_Z = \max\{2\|Z^{-1}\|, 2\}$ with Z as defined in (3.16). Then, the relative residual norm in solving (3.2) by GMRES with preconditioner (3.8) satisfies*

$$(4.14) \quad \frac{\|\hat{r}_k\|}{\|\hat{r}_0\|} \leq \min\{1, \hat{C}_Z k^k (k-2)^{2-k} (1-2\epsilon)^{k-2}\}, \text{ for } k \geq 3.$$

Furthermore, the GMRES algorithm in solving the transformed 2LM system converges to a fixed tolerance in

$$(4.15) \quad O(((1-\log \epsilon)^2)\epsilon^{-1} + \log^2 \hat{C}_Z)$$

iterations.

Proof. The residuals in GMRES algorithm satisfy the minimum residual property, i.e.,

$$\|\hat{r}_k\| = \min_{p \in \mathbb{P}_k} \|p(\hat{P}^{-1}A_{2LM})\hat{r}_0\|,$$

where $\mathbb{P}_k = \{\text{polynomials } p \text{ of degree } \leq k \text{ with } p(0) = 1\}$. This implies that $\|\hat{r}_k\| \leq \|\hat{r}_0\|$.

Let $S_{\tilde{\epsilon}}$ be the disk with center $(1/2, 0)$ and radius $1/2 - \tilde{\epsilon}$, where $0 \leq \tilde{\epsilon} < \epsilon$. Denote by $\Gamma_{\tilde{\epsilon}}$ the (circular) boundary of $S_{\tilde{\epsilon}}$ and recall the definition of $R_b(\cdot)$ in (4.9). Using estimates popular in pseudo-spectral analysis, e.g in [12], we have

$$(4.16) \quad \begin{aligned} \frac{\|\hat{r}_k\|}{\|\hat{r}_0\|} &\leq \min_{p \in \mathbb{P}_k} \|p(\hat{P}^{-1}\hat{A}_{2LM})\| \leq \min_{p \in \mathbb{P}_k} \frac{1}{2\pi} \int_{\Gamma_{\tilde{\epsilon}}} |p(z)| \|R_b(z)\| dz \\ &\leq \frac{\mathcal{L}(\Gamma_{\tilde{\epsilon}})}{2\pi} \max_{z \in \Gamma_{\tilde{\epsilon}}} \|R_b(z)\| \min_{p \in \mathbb{P}_k} \max_{z \in S_{\tilde{\epsilon}}} |p(z)|, \quad (\mathcal{L}(\Gamma_{\tilde{\epsilon}}) : \text{length of } \Gamma_{\tilde{\epsilon}}) \end{aligned}$$

$$(4.17) \quad \leq (1-\tilde{\epsilon}) \max_{z \in \Gamma_{\tilde{\epsilon}}} \|R_b(z)\| \min_{p \in \mathbb{P}_k} \max_{z \in S_{\tilde{\epsilon}}} |p(z)|$$

Since $S_{\tilde{\epsilon}}$ is a disk, according to [7], the last term in (4.17) can be estimated by

$$(4.18) \quad \min_{p \in \mathbb{P}_k} \max_{z \in S_{\tilde{\epsilon}}} |p(z)| \approx \rho^k, \text{ where } \rho = 1 - 2\tilde{\epsilon}.$$

Recalling the definition of $R_b(\cdot)$ in (4.9) and noting that for $z \in \Gamma_{\tilde{\epsilon}}$, $R_b(z)$ is large when either $z = \tilde{\epsilon}$ or $z = 1 - \tilde{\epsilon}$, we have a rough estimate for the second term in (4.17)

$$(4.19) \quad \max_{z \in \Gamma_{\tilde{\epsilon}}} \|R_b(z)\| \leq \hat{C}_Z (\tilde{\epsilon} - \epsilon)^{-2},$$

where \hat{C}_Z is defined in the statement of the theorem. From (4.17), (4.18), and (4.19), we find that

$$(4.20) \quad \frac{\|\hat{r}_k\|}{\|\hat{r}_0\|} \leq \hat{C}_Z \overbrace{\left((\tilde{\epsilon} - \epsilon)^{-2} (1 - 2\tilde{\epsilon})^k \right)}^{\rho(\epsilon, \tilde{\epsilon}, k)}.$$

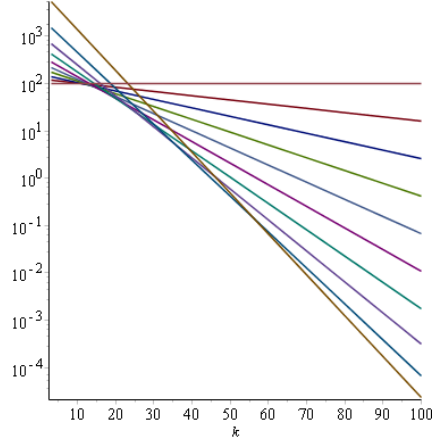


FIG. 4.1. Different upper bounds of the relative residual for different values of $\tilde{\epsilon}$.

We emphasize that this estimate is valid for all values of $0 \leq \tilde{\epsilon} < \epsilon$. Figure 4.1 shows some of these bounds for $\hat{C}_Z = 1$, $\epsilon = 0.1$. It can be noticed that in the asymptotic regime, the overall bound behaves very much like $\bar{C}_s (1 - 2\epsilon)^{k-2}$ for some constant \bar{C}_s .

Now, solving $\frac{\partial}{\partial \tilde{\epsilon}} \rho(\epsilon, \tilde{\epsilon}, k) = 0$ reveals that the best choice of $\tilde{\epsilon}$ is $\tilde{\epsilon} = \max \left\{ \frac{\epsilon k - 1}{k - 2}, 0 \right\}$. Substituting this best choice of $\tilde{\epsilon}$ into (4.20) gives (4.14).

To obtain the iteration estimate, substitute $k = k_0 = ((1 - \log \epsilon)^2 \epsilon^{-1} + \log^2 \hat{C}_Z)$ into (4.14) and obtain

$$\rho(\epsilon, \hat{C}_Z) = \frac{\hat{C}_Z}{\epsilon^2} \left(\left((1 - \log \epsilon)^2 + \epsilon \log^2 \hat{C}_Z \right)^{((1 - \log \epsilon)^2 + \epsilon \log^2 \hat{C}_Z) \epsilon^{-1}} \times \left(\frac{1 - 2\epsilon}{(1 - \log \epsilon)^2 + \epsilon (\log^2 \hat{C}_Z - 2)} \right)^{((1 - \log \epsilon)^2 + \epsilon (\log^2 \hat{C}_Z - 2)) \epsilon^{-1}} \right).$$

We have plotted $\rho(\epsilon, \hat{C}_Z)$ in Fig. 4.2. From this plot, we see that the relative residual is reduced by a factor of $\rho(\epsilon, \hat{C}_Z) < 0.01$ every k_0 iterations, as required. \square

We are now ready to give our main result on the convergence of GMRES algorithm for solving the preconditioned 2LM system (2.21).

THEOREM 4.4. *Let $C_Z = \sqrt{\kappa(B)} \max \{2\|Z^{-1}\|, 2\}$ with Z as defined in (3.16). Then, the relative residual norm in solving (2.21) by GMRES satisfies*

$$(4.21) \quad \frac{\|r_k\|}{\|r_0\|} \leq \min\{1, C_Z k^k (k - 2)^{2-k} (1 - 2\epsilon)^{k-2}\}, \text{ for } k \geq 3.$$

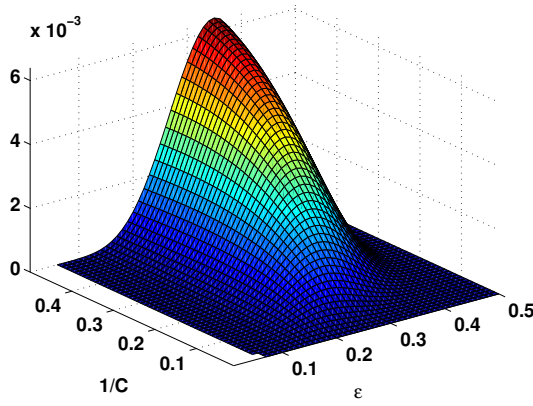


FIG. 4.2. Residual norm $\rho(\epsilon, \hat{C}_Z)$ after $k_0 = ((1 - \log \epsilon)^2)\epsilon^{-1} + \log^2 \hat{C}_Z$ iterations, as a function of ϵ and $1/\hat{C}_Z$.

Furthermore, the GMRES algorithm in 2LM method converges to a fixed tolerance in

$$(4.22) \quad O(((1 - \log \epsilon)^2)\epsilon^{-1} + \log^2 C_Z)$$

iterations.

Proof. The residual norms of GMRES in solving (2.21), satisfy the minimum residual property, namely

$$\|r_k\| = \min_{p \in \mathbb{P}_k} \|p(P^{-1}A_{2LM})r_0\|.$$

Therefore,

$$(4.23) \quad \begin{aligned} \frac{\|r_k\|}{\|r_0\|} &\leq \min_{p \in \mathbb{P}_k} \|p(P^{-1}A_{2LM})\| = \min_{p \in \mathbb{P}_k} \|p(B^{1/2}\hat{P}^{-1}\hat{A}_{2LM})B^{-1/2}\| \\ &\leq \kappa(B^{1/2}) \min_{p \in \mathbb{P}_k} \|p(\hat{P}^{-1}\hat{A}_{2LM})\| = \sqrt{\kappa(B)} \min_{p \in \mathbb{P}_k} \|p(\hat{P}^{-1}\hat{A}_{2LM})\|. \end{aligned}$$

The proof is finished using the same estimate in the proof for Theorem 4.3 for the second factor of the last term in (4.23). \square

4.1. Optimal Robin parameter. In [31, 6], all eigenvectors of (3.5) associated with eigenvalues of size less than $\text{diam}(\Omega_i)^{-1}$ are included in the coarse space. This seems to work well for all of their considered test problems. The same approach can be utilized for our proposed method. However, in our method, the rate of convergence can be estimated a priori and we should exploit this feature in determining our spectral coarse space.

Assume that the spectrum of the generalized eigenvalue problem can be decomposed as follows (3.4)

$$(4.24) \quad \sigma(S, B) = \{0 < \dots < s_0\} \cup \{s_{\min} < \dots < s_{\max}\},$$

where the coarse space is constructed using the eigenfunctions associated with eigenvalues in the set $\{0 < \dots < s_0\}$. We recall that the eigenvalues of Q are of the form

$a/(a+s)$ with $s \in \sigma(S, B)$. In addition, the spectrum of Q is $\sigma(Q) = [\epsilon, 1-\epsilon] \cup (1-\epsilon, 1]$. Therefore, it is required that

$$\frac{a}{a+s} \subset [\epsilon, 1-\epsilon], \quad \text{for } s_{\min} < s < s_{\max}.$$

Or equivalently,

$$(4.25) \quad \epsilon \leq \min \left\{ \frac{s_{\min}}{a+s_{\min}}, \frac{a}{a+s_{\max}} \right\}$$

According to Theorem 4.4, the larger ϵ is the faster the 2LM method converges. Therefore, we would like to choose a so that ϵ is largest. This happens when the two quantities on the right hand side of (4.25) equal, or

$$(4.26) \quad a_{\text{op}} = \sqrt{s_{\min}s_{\max}},$$

as one of the ratios in (4.25) is increasing and the other decreasing w.r.t a .

Consequently, the optimal value of ϵ is

$$(4.27) \quad \epsilon_{\text{op}} = \frac{1}{1 + \sqrt{\kappa_{\text{eff}}(S)}}, \quad \text{where } \kappa_{\text{eff}}(S) = \frac{s_{\max}}{s_{\min}}.$$

Since we only need s_{\min} and s_{\max} to determine ϵ , the convergence rate of our method can be obtained a priori. If the rate of convergence is not as good as expected, more eigenvectors can be added to the coarse space.

4.2. Convergence estimate in term of mesh parameters. Although we cannot estimate the norm of the coarse problem $\|Z^{-1}\|$ and thus \hat{C}_Z when we have no information about the coarse space, it is worthwhile discussing what the estimate (4.14) reveals about the classical case where the coarse space consists of piecewise constant functions and where the problem is homogeneous, with benign variations in the diffusion coefficient (or even in the case where the elliptic problem is the Laplacian).

In this case, the condition number of the local Schur complement S (modulo the coarse space of constant functions) is $O(H/h)$, yielding the value $\epsilon^{-1} = O(\sqrt{H/h})$; and $\hat{C}_Z = 2\|(I - 2K_{22})\hat{Q}_2 + K_{22}\|^{-1} = 2\|(I - K_{22})^{-1}\| = O(H^{-2})$ [24]. As a result, the iteration count estimate (4.15) becomes

$$(4.28) \quad O(\sqrt{H/h} \log^2 \sqrt{H/h} + \log^2(H)) \text{ iterations,}$$

which is consistent with the Fourier analysis done in [11].

The above analysis also applies to the heterogeneous case where the diffusion coefficient is “quasi-monotone” [33]. Recall that the diffusion coefficient $\alpha(x)$ is quasi-monotone, roughly, if for any $x \in \Omega$ there is a path $\gamma(t)$ from x to $y = \operatorname{argmax}_x \alpha(x)$ such that $\alpha(\gamma(t))$ is monotonically increasing. In that situation, the generalized condition number of the pencil (S, B) , modulo the coarse space of piecewise constant functions, is also $O(H/h)$ and the estimate is again (4.28).

If the diffusion coefficient is heterogeneous and not quasi-monotone then the pencil (S, B) is likely to have some extreme eigenvalues apart from those related to the kernel of S . In that case, using a “classical” coarse space gives very slow convergence. Our new spectral coarse space automatically adapts to this difficult heterogeneous case and gives arbitrarily good convergence by automatically enriching the coarse space.

5. Numerical Experiments. In this section, we will use our proposed method to solve the model problem (2.1) for different types of variation in the coefficient α . The considered types of α are similar to the ones in [31].

In all of the experiments, the domain Ω is the unit square $\Omega = (0, 1)^2$. We use uniform triangular meshes of size $h = 1/64, 1/128, 1/256$. Unless stated otherwise, the regular tile partitions $4 \times 4, 8 \times 8$ and 16×16 will be considered.

The transformed 2LM system (3.13) is solved by GMRES algorithm [38] with relative residual tolerance of 10^{-9} and maximum number of iterations of n_Γ or 500, whatever is smaller (n_Γ is the size of the 2LM systems). We consider three cases: without any preconditioner, with the two-level preconditioner P_0 in [25] and with our preconditioner \hat{P} in (3.8). The λ obtained from $\hat{\lambda}$ is used as data for the local discrete problems (2.8). These are solved directly to obtain u , the approximation of the discrete solution. We will report the number of GMRES iterations in solving (3.13) for the Lagrange multiplier $\hat{\lambda}$, and the relative error of the approximation of the discrete solution $\frac{\|u - u_{ex}\|}{\|u_{ex}\|}$, where u_{ex} is computed by a direct solver. We will also provide “dim”, the dimension of the coarse space and the value of parameter ϵ for the case with preconditioner \hat{P} . In all of the experiments, we will start with

$$\text{dim} = \min \left\{ \max \{4p, \text{round}(0.1n_\Gamma)\}, \text{round}(0.2n_\Gamma) \right\}$$

and increase “dim” (through adding more eigenfunctions to the coarse space) by $0.05n_\Gamma$ if $\epsilon < 0.1$.

For the last three experiments, the configuration with $h = 1/64$ and partition 4×4 is more thoroughly studied. We plot eigenvalues of the generalized eigenvalue problem (3.4), the spectrum of the preconditioned system $\hat{P}^{-1}\hat{A}_{2LM}$ and the convergence history of solving (3.13) by GMRES. A plot of $C_s(1 - 2\epsilon)^{k-2}$ for a suitable C_s is provided along the convergence history for comparison.

5.1. Continuous Variations of the Coefficient. In this experiments, we consider a continuous function $\alpha_c(x)$, where

$$\log_{10}(\alpha_c(x)) = \kappa \sin(w\pi(x(1) + x(2))),$$

with $\kappa = 3$, $w = 4$ and $x(i)$ is the i th coordinate of x . The coefficient $\alpha(x)$ is a

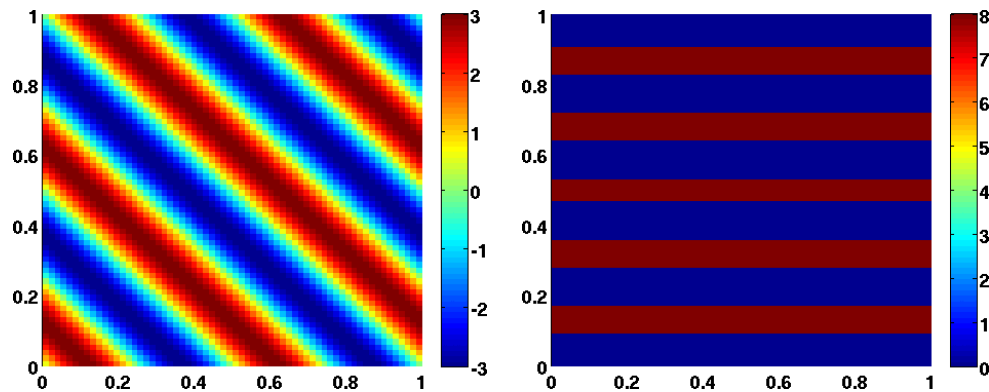


FIG. 5.1. $\log_{10}(\alpha(x))$ in the continuous test case (left) and alternating test case (right).

piecewise constant approximation of $\alpha_c(x)$ with interpolation points at the centroids of elements. The contrast ratio in this experiment is 10^6 . Figure 5.1-left shows $\log_{10}(\alpha(x))$ on the uniform mesh of size $1/64$ for the continuous test case.

TABLE 5.1
Convergence in continuous test case.

p	No Preconditioner		Preconditioner \hat{P}			
	Its.	$\frac{\ u-u_{ex}\ }{\ u_{ex}\ }$	Its.	$\frac{\ u-u_{ex}\ }{\ u_{ex}\ }$	dim	ϵ
$h^{-1} = 64$						
16	76	4.5e-8	21	2.1e-10	128	2.56e-1
64	134	2.5e-8	24	9.3e-11	353	2.67e-1
256	265	7.6e-1	25	3.2e-10	756	2.62e-1
$h^{-1} = 128$						
16	88	4.0e-9	21	9.3e-11	229	2.78e-1
64	157	9.4e-9	22	3.1e-10	533	2.74e-1
256	288	1.2e-8	21	9.3e-10	1524	3.02e-1
$h^{-1} = 256$						
16	106	6.3e-9	18	1.9e-10	459	2.82e-1
64	193	1.1e-9	18	6.3e-10	1071	2.83e-1
256	337	8.8e-9	22	2.2e-10	2295	2.83e-1

In table 5.1, we can see that the preconditioner \hat{P} helps to substantially reduce the number of GMRES iterations while delivering better accuracy for the approximation of the discrete solution. The convergence rate (which is a function of ϵ) and consequently the iteration count in the preconditioned case are stable with respect to changes in the mesh size h and the number of subdomains p . The size of the coarse space does grow as h becomes smaller and p becomes bigger. However, this is inevitable as the problem becomes harder and the coarse space must adapt to maintain a reasonable iteration count.

5.2. Highly Heterogeneous Coefficient: Alternating Case. We consider the case where the coefficient α alternates between 1 and 10^8 in eleven horizontal stripes (cf. Figure 5.1-right). More precisely, $\alpha|_{\tau} = 10^8$ if every point x in τ satisfies

$$\text{mod}(\text{floor}(11x(2)), 2) = 1,$$

and $\alpha_{\tau} = 1$ otherwise. Here “mod” and “floor” denotes the modulo and rounding (to the nearest integer towards minus infinity) operators, respectively. The contrast ratio in this experiment is 10^8 .

In Table 5.2, \hat{P} shows a performance similar to that in the continuous test case. It requires small, stable number of iterations while delivering better accuracy.

5.3. Highly Heterogeneous Coefficient: Skyscraper Case. In this experiment, we consider

$$\alpha|_{\tau} = 10^{2*\text{mod}(\text{floor}(10cx_{\tau}(1)), 2)-1}, \quad cx_{\tau} \text{ is the centroid of } \tau$$

if every point x of τ satisfies

$$\text{mod}(\text{floor}(10x(i)), 2) = 1, \quad i = 1, 2.$$

TABLE 5.2
Convergence in alternating test case.

p	No Preconditioner		Preconditioner \hat{P}			
	Its.	$\frac{\ u-u_{ex}\ }{\ u_{ex}\ }$	Its.	$\frac{\ u-u_{ex}\ }{\ u_{ex}\ }$	dim	ϵ
$h^{-1} = 64$						
16	70	3.1e-8	16	1.6e-10	128	3.08e-1
64	148	2.0e-8	18	4.8e-10	353	3.24e-1
256	214	9.3e-9	24	5.8e-10	756	2.98e-1
$h^{-1} = 128$						
16	88	1.7e-8	17	7.1e-11	229	2.95e-1
64	157	2.2e-8	20	2.0e-10	533	2.95e-1
256	337	7.1e-9	20	3.0e-10	1524	3.12e-1
$h^{-1} = 256$						
16	108	1.2e-8	16	1.2e-10	459	2.98e-1
64	198	1.1e-8	17	2.3e-10	1071	2.95e-1
256	402	9.5e-9	20	2.3e-10	2295	2.96e-1

Figure 5.2-left shows $\log_{10}(\alpha)$ for the skyscraper test case. Basically, in the islands, we have $\alpha = 10^{(2k-1)}$, $k = 1, \dots, 5$ from left to right. In the rest of the domain, $\alpha = 1$. The contrast ratio in this experiment is 10^9 .

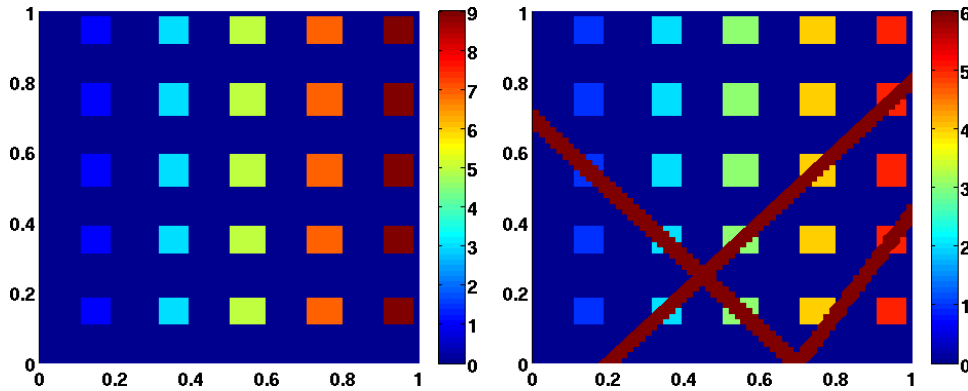


FIG. 5.2. $\log_{10}(\alpha(x))$ in the skyscraper test case (left) and channels and inclusions test case (right).

According to Table 5.3, in this test case, the equation (3.13) is very difficult to solve without a preconditioner. In many cases, the desired tolerance of 10^{-9} can not be achieved even after the maximum GMRES iterations $\min\{n_T, 500\}$. Consequently, the computed discrete solutions are inaccurate with relative errors often bigger than 10^{-2} . On the other hand, the preconditioner \hat{P} keeps the number of GMRES iterations below 21. The computed discrete solutions are also fairly accurate with relative errors of around 10^{-6} . We also do not see big changes in iteration count as the mesh size

TABLE 5.3
Convergence in skyscraper test case.

p	No Preconditioner		Preconditioner \hat{P}			
	Its.	$\frac{\ u-u_{ex}\ }{\ u_{ex}\ }$	Its.	$\frac{\ u-u_{ex}\ }{\ u_{ex}\ }$	dim	ϵ
$h^{-1} = 64$						
16	301	2.7e-2	21	3.7e-6	128	1.74e-1
64	442	3.7e-2	19	3.8e-6	353	2.33e-1
256	500	7.6e-1	19	2.1e-6	756	2.16e-1
$h^{-1} = 128$						
16	457	1.7e-2	20	6.4e-6	229	1.67e-1
64	500	5.2e-2	19	2.2e-6	533	1.98e-1
256	500	8.8e-1	18	1.7e-6	1524	2.41e-1
$h^{-1} = 256$						
16	500	1.1e-0	17	2.5e-5	459	1.70e-1
64	500	8.9e-1	16	6.7e-6	1071	2.01e-1
256	500	1.0e-0	15	4.1e-6	2295	2.16e-1

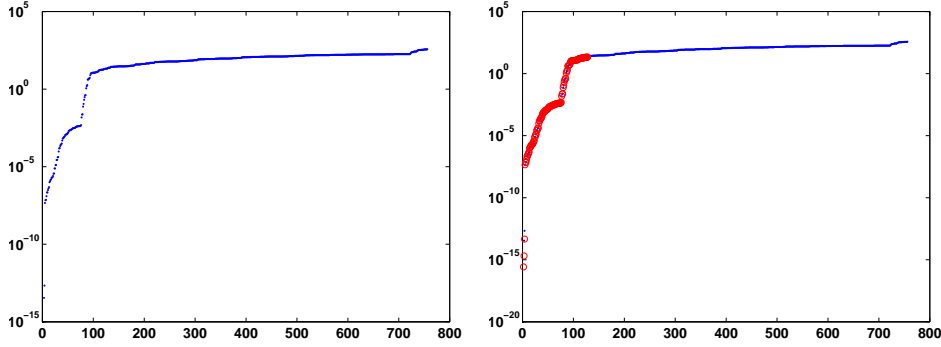


FIG. 5.3. Skyscraper: plots of eigenvalues of the generalized eigenvalue problem (3.4) with the selected ones for the coarse space marked by circles in red on the right.

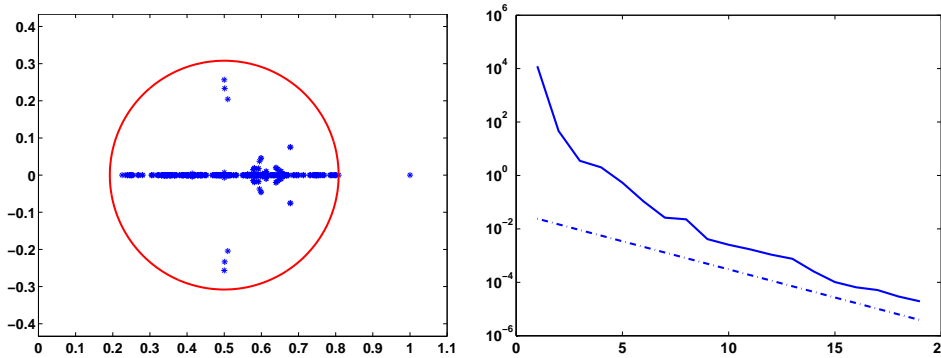


FIG. 5.4. Skyscraper: spectrum of $\hat{P}^{-1}\hat{A}_{2LM}$ (left) and convergence history with predicted rate of convergence (slope of the dotted line) in solving $\hat{P}^{-1}\hat{A}_{2LM}\hat{\lambda} = -\hat{P}^{-1}(I - 2K)\hat{Q}\hat{g}$ (right).

and the number of subdomains vary.

For the case study, where $h = 1/64$ and $p = 16$, the eigenvalues of the generalized eigenvalue problem are plotted in Figure 5.3 with the ones selected for the coarse space marked by circles in red on the right. The number of selected eigenvalues is small compared to the size of the 2LM system. The spectrum of $\hat{P}^{-1}\hat{A}_{2LM}$ is illustrated in Figure 5.4 (left). We can see that all of the eigenvalues lie inside the circle S_ϵ as proved by Lemma 4.1. The convergence history and predicted rate of convergence (dashed-dotted line) is shown in Figure 5.4 (right). It can be seen that the rate of convergence agrees with the prediction in Theorem 4.3.

5.4. Channels and Inclusions. The set up for the coefficient α in this experiment is similar to the one in subsection 5.3 with $\alpha = 10^k$, $k = 1, \dots, 5$ in the islands from left to right. In addition, there are three channels with $\alpha = 10^6$ (see Figure 5.2-right). The contrast ratio of the coefficient α in this experiment is 10^6 . This is a test problem with known difficulties for many common preconditioners.

In this experiment, we also compare our new preconditioner \hat{P} with the more classical preconditioner P_0 based on a piecewise constant coarse space [25]. Due to limited space, we omit the coarse space dimensions. They are actually the same as in the previous experiments.

From Table 5.4, it can be seen that P_0 only helps to reduce the GMRES iteration count minimally, and that its performance and accuracy quickly deteriorate when p increases. Our preconditioner \hat{P} , on the other hand, keeps the iteration count stable and reasonably small while delivering superior accuracy.

For the case study, where $h = 1/64$ and $p = 16$, the eigenvalues of the generalized eigenvalue problem are plotted in Figure 5.5. The spectrum of the preconditioned system in Figure 5.6 (left) and the convergence history in Figure 5.6 (right) agree with Lemma 4.1 and Theorem 4.3, respectively.

TABLE 5.4
Convergence in channels and inclusions test case.

p	No Preconditioner		Preconditioner P_0		Preconditioner \hat{P}		
	Its.	$\frac{\ u-u_{ex}\ }{\ u_{ex}\ }$	Its.	$\frac{\ u-u_{ex}\ }{\ u_{ex}\ }$	Its.	$\frac{\ u-u_{ex}\ }{\ u_{ex}\ }$	ϵ
$h^{-1} = 64$							
16	205	1.4e-6	185	1.4e-5	32	3.0e-8	1.84e-1
64	332	1.2e-6	224	1.3e-2	30	2.3e-8	2.28e-1
256	500	9.0e-2	500	3.6e-1	36	2.6e-8	2.08e-1
$h^{-1} = 128$							
16	299	3.4e-7	185	1.4e-5	33	2.4e-8	1.73e-1
64	414	2.9e-7	239	4.6e-3	35	1.4e-8	2.01e-1
256	500	1.9e-2	500	1.6e-1	30	1.2e-8	2.41e-1
$h^{-1} = 256$							
16	408	2.3e-7	377	6.9e-6	37	1.4e-8	1.74e-1
64	498	1.6e-7	302	1.4e-3	30	6.2e-9	2.06e-1
256	500	5.9e-2	500	1.3e-1	30	1.0e-8	2.16e-1

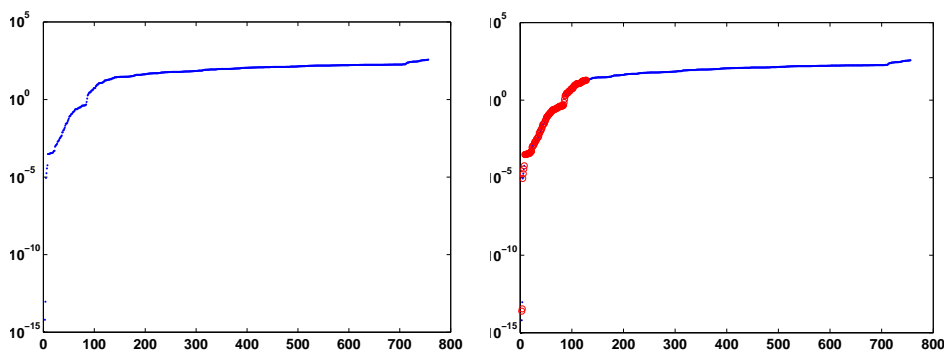


FIG. 5.5. Channels and inclusions: plots of eigenvalues of the generalized eigenvalue problem (3.4) with the selected ones for the coarse space marked by circles in red on the right.

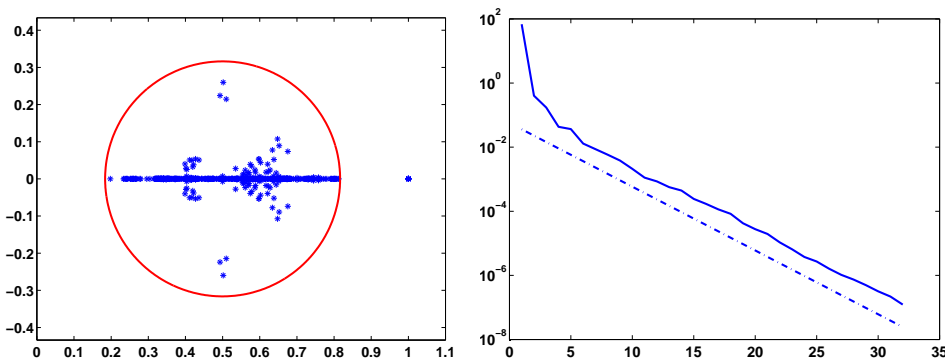


FIG. 5.6. Channels and inclusions: spectrum of $\hat{P}^{-1}\hat{A}_{2LM}$ (left) and convergence history with predicted rate of convergence (slope of the dotted line) in solving $\hat{P}^{-1}\hat{A}_{2LM}\hat{\lambda} = -\hat{P}^{-1}(I - 2K)\hat{Q}\hat{g}$ (right).

5.5. Lognormal. In this experiment, $\alpha = \alpha(x, w) = 10^{Z(x, w)}$, where $Z(x, w)$ is a Gaussian random field with zero mean and Gaussian covariance

$$C(x, y) = \sigma^2 \exp\left(-\frac{\|x - y\|^2}{\ell^2}\right), \quad \text{with } \sigma = 1, \ell^2 = 1e-3.$$

Our realization of α is generated by the spectral decomposition method described in [28]. An example of $\log_{10}(\alpha)$ for the mesh of size $1/128$ is shown in Figure 5.7-left. The contrast ratio in this example is 10^8 .

Similar to the channels and inclusions test case 5.4, the preconditioner P_0 only helps to reduce the GMRES iteration count minimally (cf. Table 5.5). Its performance and accuracy quickly deteriorate when p increases. Our preconditioner \hat{P} , on the other hand, keeps the iteration count stable and small while delivering good accuracy. It is also robust with the changes in mesh size and number of subdomains. The coarse space dimensions are again the same as in the first three test cases.

For the case study, where $h = 1/64$ and $p = 16$, the eigenvalues of the generalized eigenvalue problem are plotted in Figure 5.3. The spectrum of the preconditioned

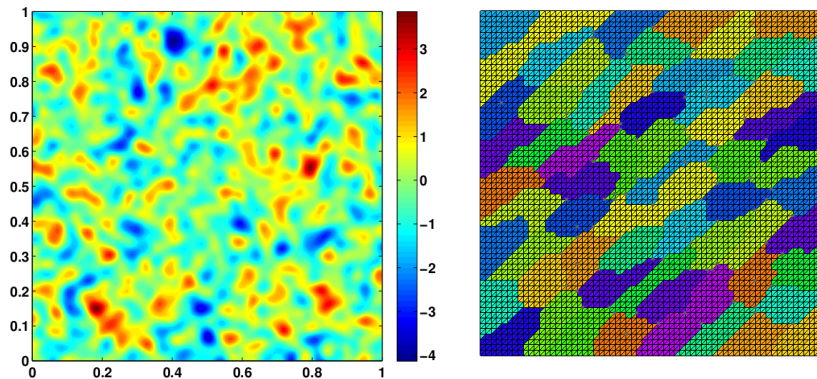


FIG. 5.7. $\log_{10}(\alpha(x))$ in the lognormal test case (left) and a partition generated by Metis (right).

TABLE 5.5
Convergence in lognormal test case.

p	No Preconditioner		Preconditioner P_0		Preconditioner \hat{P}		
	Its.	$\frac{\ u-u_{ex}\ }{\ u_{ex}\ }$	Its.	$\frac{\ u-u_{ex}\ }{\ u_{ex}\ }$	Its.	$\frac{\ u-u_{ex}\ }{\ u_{ex}\ }$	ϵ
$h^{-1} = 64$							
16	99	1.5e-9	66	3.3e-4	23	1.2e-9	2.65e-1
64	161	1.5e-9	113	2.1e-3	23	2.1e-9	2.79e-1
256	500	7.6e-1	308	1.7e-2	19	2.1e-6	2.16e-1
$h^{-1} = 128$							
16	128	2.8e-9	74	6.2e-5	23	2.0e-9	2.40e-1
64	216	1.5e-9	141	2.9e-4	28	4.5e-9	2.22e-1
256	451	7.9e-10	372	1.2e-2	27	4.0e-9	2.46e-1
$h^{-1} = 256$							
16	158	1.5e-9	102	7.6e-6	20	3.4e-9	2.59e-1
64	267	7.9e-9	159	1.4e-4	21	3.4e-9	2.58e-1
256	500	3.0e-9	367	1.3e-3	23	3.5e-9	2.50e-1

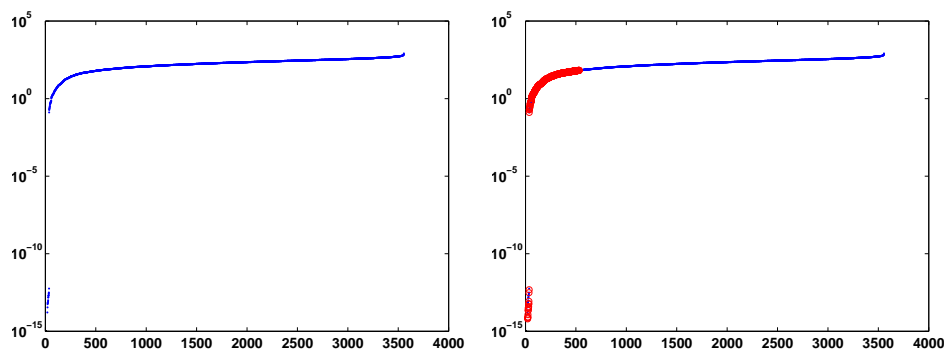


FIG. 5.8. Lognormal: plots of eigenvalues of the generalized eigenvalue problem (3.4) with the selected ones for the coarse space marked by circles in red on the right.

system and the convergence history shown in Figure 5.9 agrees with Lemma 4.1 and Theorem 4.3, respectively.

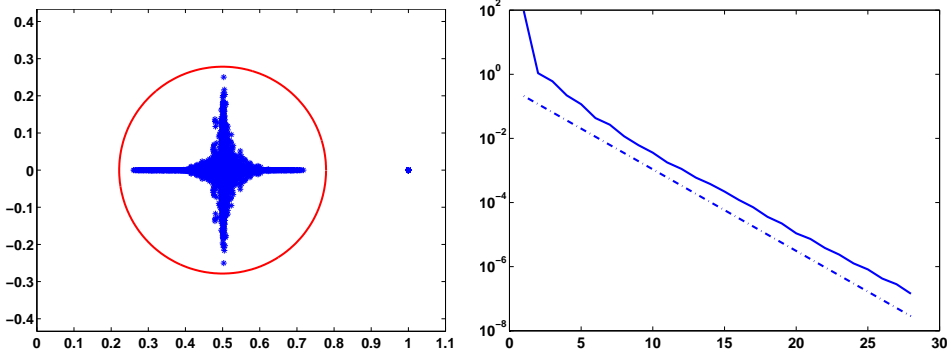


FIG. 5.9. Lognormal: spectrum of $\hat{P}^{-1}\hat{A}_{2LM}$ (left) and convergence history with predicted rate of convergence (slope of the dotted line) in solving $\hat{P}^{-1}\hat{A}_{2LM}\hat{\lambda} = -\hat{P}^{-1}(I - 2K)\hat{Q}\hat{g}$ (right).

In order to make sure that our preconditioner works for general partitions, we use Metis [22] to generate the partitions used in our last test (see Table 5.6). Figure 5.7-right shows the partition for the mesh with $h = 1/64$ and $p = 64$.

The preconditioner \hat{P} is still the winner with good accuracy and much smaller iteration count. In comparison with the case where regular partitions are used, the iteration counts are bigger especially when the mesh is coarse ($h = 1/64$). However, they become reasonably small for finer meshes.

TABLE 5.6
Convergence in lognormal test case with Metis partitions.

p	No Preconditioner		Preconditioner P_0		Preconditioner \hat{P}		
	Its.	$\frac{\ u-u_{ex}\ }{\ u_{ex}\ }$	Its.	$\frac{\ u-u_{ex}\ }{\ u_{ex}\ }$	Its.	$\frac{\ u-u_{ex}\ }{\ u_{ex}\ }$	ϵ
$h^{-1} = 64$							
16	130	9.7e-10	80	1.0e-4	39	4.9e-9	1.53e-1
64	202	1.1e-9	155	3.5e-4	46	6.9e-9	1.51e-1
256	390	8.2e-10	463	3.9e-3	64	1.2e-8	8.65e-2
$h^{-1} = 128$							
16	156	1.1e-9	112	1.6e-5	30	5.9e-9	1.91e-1
64	249	9.0e-10	186	1.9e-4	32	8.1e-9	1.84e-1
256	465	1.1e-9	454	4.7e-3	33	9.0e-9	1.68e-1
$h^{-1} = 256$							
16	181	1.5e-9	133	2.0e-6	22	5.2e-9	2.25e-1
64	294	7.9e-10	192	1.1e-4	25	4.7e-9	2.10e-1
256	500	9.1e-9	478	1.3e-3	27	5.8e-9	2.19e-1

6. Conclusion. We have formulated and analyzed a two-level preconditioner for optimized Schwarz and 2-Lagrange methods. With a coarse space that can automatically adapt to diffusion coefficient and achieve any a priori given linear rate of

convergence, our preconditioner is very efficient and robust with highly heterogeneous diffusion coefficient. Numerical results have verified our theoretical findings.

REFERENCES

- [1] J. AARNES AND T. Y. HOU, *Multiscale domain decomposition methods for elliptic problems with high aspect ratios*, Acta Math. Appl. Sin. Engl. Ser., 18 (2002), pp. 63–76.
- [2] H. BERNINGER, S. LOISEL, AND O. SANDER, *The 2-lagrange multiplier method applied to nonlinear transmission problems for the Richards equation in heterogeneous soil with cross points*, SIAM J. Sci. Comput., (to appear).
- [3] E. J. BRAGA AND M. J. DE LEMOS, *Heat transfer in enclosures having a fixed amount of solid material simulated with heterogeneous and homogeneous models*, Int. J. Heat. Mass. Tran., 48 (2005), pp. 4748–4765.
- [4] T. F. CHAN AND T. P. MATHEW, *Domain decomposition algorithms*, Acta numerica, 3 (1994), pp. 61–143.
- [5] K. CLIFFE, I. G. GRAHAM, R. SCHEICHL, AND L. STALS, *Parallel computation of flow in heterogeneous media modelled by mixed finite elements*, J. Comput. Phys., 164 (2000), pp. 258–282.
- [6] V. DOLEAN, F. NATAF, R. SCHEICHL, AND N. SPILLANE, *Analysis of a two-level Schwarz method with coarse spaces based on local Dirichlet-to-Neumann maps*, Comput. Methods Appl. Math., 12 (2012), pp. 391–414.
- [7] T. A. DRISCOLL, K.-C. TOH, AND L. N. TREFETHEN, *From potential theory to matrix iterations in six steps*, SIAM review, 40 (1998), pp. 547–578.
- [8] S. W. DRURY AND S. LOISEL, *Sharp condition number estimates for the symmetric 2-lagrange multiplier method*, in Domain Decomposition Methods in Science and Engineering XX, Springer, 2013, pp. 255–261.
- [9] M. DRYJA, M. V. SARKIS, AND O. B. WIDLUND, *Multilevel schwarz methods for elliptic problems with discontinuous coefficients in three dimensions*, Numer. Math., 72 (1996), pp. 313–348.
- [10] M. DRYJA, B. F. SMITH, AND O. B. WIDLUND, *Schwarz analysis of iterative substructuring algorithms for elliptic problems in three dimensions*, SIAM J. Numer. Anal., 31 (1994), pp. 1662–1694.
- [11] O. DUBOIS, M. J. GANDER, S. LOISEL, A. ST-CYR, AND D. B. SZYLD, *The optimized Schwarz method with a coarse grid correction*, SIAM J. Sci. Comput., 34 (2012), pp. A421–A458.
- [12] M. EMBREE, *How descriptive are gmres convergence bounds?*, (1999).
- [13] C. FARHAT, A. MACEDO, M. LESOINNE, F.-X. ROUX, F. MAGOULÉS, AND A. D. L. BOURDONNAIE, *Two-level domain decomposition methods with lagrange multipliers for the fast iterative solution of acoustic scattering problems*, Comput. Method Appl. M., 184 (2000), pp. 213–239.
- [14] C. FARHAT AND F.-X. ROUX, *A method of finite element tearing and interconnecting and its parallel solution algorithm*, Internat. J. Numer. Methods Engrg., 32 (1991), pp. 1205–1227.
- [15] J. GALVIS AND Y. EFENDIEV, *Domain decomposition preconditioners for multiscale flows in high-contrast media*, Multiscale Model. Sim., 8 (2010), pp. 1461–1483.
- [16] ———, *Domain decomposition preconditioners for multiscale flows in high contrast media: reduced dimension coarse spaces*, Multiscale Model. Sim., 8 (2010), pp. 1621–1644.
- [17] M. J. GANDER, *Optimized Schwarz methods*, SIAM J. Numer. Anal., 44 (2006), pp. 699–731.
- [18] M. J. GANDER, L. HALPERN, AND F. NATAF, *Optimized Schwarz methods*, in Domain decomposition methods in sciences and engineering (Chiba, 1999), DDM.org, Augsburg, 2001, pp. 15–27 (electronic).
- [19] I. G. GRAHAM AND M. J. HAGGER, *Unstructured additive Schwarz-conjugate gradient method for elliptic problems with highly discontinuous coefficients*, SIAM J. Sci. Comput., 20 (1999), pp. 2041–2066.
- [20] I. G. GRAHAM, P. O. LECHNER, AND R. SCHEICHL, *Domain decomposition for multiscale PDEs*, Numer. Math., 106 (2007), pp. 589–626.
- [21] A. KARANGELIS, S. LOISEL, AND C. MAYNARD, *Solving large systems on hector using the 2-lagrange multiplier methods*, in Domain decomposition methods in science and engineering XXI, to appear.
- [22] G. KARYPIS AND V. KUMAR, *A software package for partitioning unstructured graphs, partitioning meshes, and computing fill-reducing orderings of sparse matrices*, University of Minnesota, Department of Computer Science and Engineering, Army HPC Research Center, Minneapolis, MN, (1998).
- [23] A. KLAWONN AND O. B. WIDLUND, *Dual and dual-primal FETI methods for elliptic problems*

- with discontinuous coefficients in three dimensions, in Domain decomposition methods in sciences and engineering (Chiba, 1999), DDM.org, Augsburg, 2001, pp. 29–39 (electronic).
- [24] S. LOISEL, *Condition number estimates for the nonoverlapping optimized Schwarz method and the 2-Lagrange multiplier method for general domains and cross points*, SIAM J. Numer. Anal., 51 (2013), pp. 3062–3083.
- [25] ———, *Condition number estimates and weak scaling for 2-level 2-lagrange multiplier methods for general domains and cross points*, SIAM J. Numer. Anal., (in press).
- [26] S. LOISEL AND D. B. SZYLD, *On the convergence of optimized Schwarz methods by way of matrix analysis*, in Domain decomposition methods in science and engineering XVIII, vol. 70 of Lect. Notes Comput. Sci. Eng., Springer, Berlin, 2009, pp. 363–370.
- [27] ———, *On the geometric convergence of optimized Schwarz methods with applications to elliptic problems*, Numer. Math., 114 (2010), pp. 697–728.
- [28] G. J. LORD, C. E. POWELL, AND T. SHARDLOW, *An Introduction to Computational Stochastic PDEs*, Cambridge Texts in Applied Mathematics, 2014.
- [29] J. MANDEL AND C. R. DOHRMANN, *Convergence of a balancing domain decomposition by constraints and energy minimization*, Numer. Linear. Algebr., 10 (2003), pp. 639–659.
- [30] T. P. A. MATHEW, *Domain decomposition methods for the numerical solution of partial differential equations*, vol. 61, Springer, 2008.
- [31] F. NATAF, H. XIANG, V. DOLEAN, AND N. SPILLANE, *A coarse space construction based on local Dirichlet-to-Neumann maps*, SIAM J. Sci. Comput., 33 (2011), pp. 1623–1642.
- [32] C. PECHSTEIN AND R. SCHEICHL, *Analysis of FETI methods for multiscale PDEs*, Numer. Math., 111 (2008), pp. 293–333.
- [33] ———, *Weighted poincaré inequalities*, IMA J. Numer. Anal., 33 (2013), pp. 652–686.
- [34] A. QADDOURI, L. LAAYOUNI, S. LOISEL, J. CÔTÉ, AND M. J. GANDER, *Optimized Schwarz methods with an overset grid for the shallow-water equations: preliminary results*, Appl. Numer. Math., 58 (2008), pp. 459–471.
- [35] R. QIAO AND P. HE, *Simulation of heat conduction in nanocomposite using energy-conserving dissipative particle dynamics*, Molecular Simulation, 33 (2007), pp. 677–683.
- [36] A. QUARTERONI AND A. VALLI, *Domain decomposition methods for partial differential equations*, Numerical Mathematics and Scientific Computation, The Clarendon Press, Oxford University Press, New York, 1999. Oxford Science Publications.
- [37] F.-X. ROUX, F. MAGOULÈS, S. SALMON, AND L. SERIES, *Optimization of interface operator based on algebraic approach*, in Domain decomposition methods in science and engineering, Natl. Auton. Univ. Mex., México, 2003, pp. 297–304 (electronic).
- [38] Y. SAAD AND M. H. SCHULTZ, *GMRES: a generalized minimal residual algorithm for solving nonsymmetric linear systems*, SIAM J. Sci. Statist. Comput., 7 (1986), pp. 856–869.
- [39] R. SCHEICHL AND E. VAINIKKO, *Additive Schwarz with aggregation-based coarsening for elliptic problems with highly variable coefficients*, Computing, 80 (2007), pp. 319–343.
- [40] R. SCHEICHL, P. S. VASSILEVSKI, AND L. T. ZIKATANOV, *Weak approximation properties of elliptic projections with functional constraints*, Multiscale Model. Sim., 9 (2011), pp. 1677–1699.
- [41] ———, *Multilevel methods for elliptic problems with highly varying coefficients on nonaligned coarse grids*, SIAM J. Numer. Anal., 50 (2012), pp. 1675–1694.
- [42] N. SPILLANE, V. DOLEAN, P. HAURET, F. NATAF, C. PECHSTEIN, AND R. SCHEICHL, *A robust two-level domain decomposition preconditioner for systems of PDEs*, C. R. Math. Acad. Sci. Paris, 349 (2011), pp. 1255–1259.
- [43] N. SPILLANE, V. DOLEAN, P. HAURET, F. NATAF, C. PECHSTEIN, AND R. SCHEICHL, *Abstract robust coarse spaces for systems of PDEs via generalized eigenproblems in the overlaps*, Numer. Math., 126 (2014), pp. 741–770.
- [44] N. SPILLANE, V. DOLEAN, P. HAURET, F. NATAF, AND D. J. RIXEN, *Solving generalized eigenvalue problems on the interfaces to build a robust two-level FETI method*, C. R. Math. Acad. Sci. Paris, 351 (2013), pp. 197–201.
- [45] A. F. TOMPSON AND L. W. GELHAR, *Numerical simulation of solute transport in three-dimensional, randomly heterogeneous porous media*, Water Resour. Res., 26 (1990), pp. 2541–2562.
- [46] A. TOSELLI AND O. WIDLUND, *Domain decomposition methods—algorithms and theory*, vol. 34 of Springer Series in Computational Mathematics, Springer-Verlag, Berlin, 2005.
- [47] J. XU AND Y. ZHU, *Uniform convergent multigrid methods for elliptic problems with strongly discontinuous coefficients*, Math. Models Methods Appl. Sci., 18 (2008), pp. 77–105.
- [48] Y. ZHU, *Domain decomposition preconditioners for elliptic equations with jump coefficients*, Numer. Linear. Algebr., 15 (2008), pp. 271–289.